

Conditions for resonant optical tunnelling in three-layer photonic microsystems

Yago Arosa, Alejandro Doval and Raúl de la Fuente

Instituto de materiais da USC - iMATUS, Grupo de Nanomateriais, Fotónica e Materia Branda, Departamento de Física Aplicada, Universidade de Santiago de Compostela, E-15782, Santiago de Compostela, Spain

Abstract: This work focuses on optical tunneling across thin three-layer planar structures embedded in a thick and transparent dielectric medium. First, compact transmittance expressions for different configurations are obtained using a generalized Fresnel coefficient method. These expressions are subsequently used to analyze various tunnelling outcomes. We show that two types of tunneling effects can be distinguished, depending on the kind of waves that are present in the core layer. When harmonic waves propagate in this layer, the transmittance formula and the phase condition for resonant tunneling are identical to that obtained in a Fabry-Perot etalon. However, in the case of evanescent or damped waves in the core layer, the new expression for transmittance provides another resonant condition related, this time, to the wave amplitude. For clarity, transparent materials are addressed first (including ideal metals), and the implications of absorption are studied later. Different angular-spectral maps are displayed to exemplify the main features of the tunneling effect in each analyzed configuration. To highlight, it is shown that tunnelling can occur in photonic systems with thicknesses up to several wavelengths.

Keywords: optical tunnelling, multilayers, photonic microcavities, transmission resonances, evanescent waves

Optical tunnelling (OT) refers to unexpected light transmission across an optical system composed mainly of high reflection components. Although this concept is relatively modern, since it emerges from the analogy with the quantum tunnel effect ¹⁻⁴, some configurations in which OT arises have been known for a long time. The most notorious, widely known since the time of Newton, is frustrated total internal reflection (FTIR) ⁵. At large incidence angles, a dielectric prism in contact with air totally reflects the transmitted light,

while an evanescent tail of the electromagnetic signal crosses the prism-air interface. When a similar prism is approached to the first one, this tail penetrates the second prism and produces a weak transmission of light that increases if the two prisms are brought closer. In more recent times (at the end of the 19th century), Charles Fabry and Alfred Perot invented an interferometer that bears their names⁶, consisting of two closely spaced plane-parallel mirrors (e.g., two metallic films). Despite the high reflectivity of the mirrors, the system allows light transmission when a singular or resonant condition is fulfilled. In this second case, in contrast to FTIR, we refer to this phenomenon as resonant OT.

New optical configurations for resonant OT have recently been proposed and studied, inspired by the optical-quantum analogy, and thus leading to possible applications in both fields. The simplest possible configurations correspond to three-layer systems, composed of a thin core layer sandwiched between two outer layers exhibiting high reflectance. Different structures can be distinguished depending on whether the layers are made of dielectric (D) or metallic (M) materials. Namely, DDD⁷⁻⁹, DMD⁷⁻¹⁰ and MDM¹¹⁻¹³ structures have been investigated. More complex systems for resonant OT include both multilayers of low- and high-refractive-index media forming either photonic crystals or one-dimensional metamaterials¹⁴⁻¹⁷ and structured metals^{18,19}. Similarly, extraordinary transmission has been observed in a single metallic layer patterned with periodic holes^{20,21} or with dielectric spheres²².

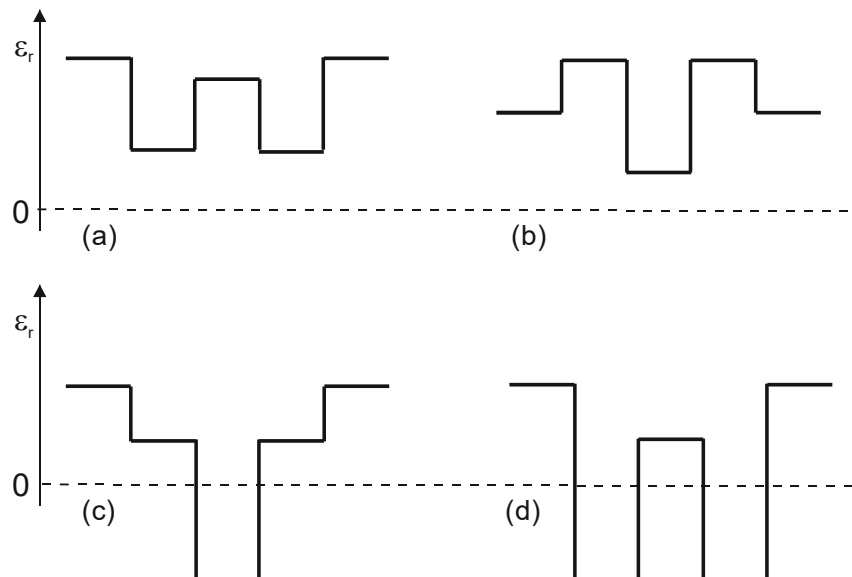


Fig. 1. Some symmetric three-layer configurations embedded in a thick surrounding dielectric that support resonant OT. The vertical axis corresponds to the relative electrical permittivity, which is assumed to be real. We can identify each configuration by its composition. We denote dielectrics with letter L or H, in relation to the low (L) or high (H)

value of their refractive index. Ideal metals are labelled as M, and they are characterized by a negative permittivity, i.e. $\varepsilon_r = n^2 = -n''^2$. Using this notation, the different configurations to be studied are: (a) LHL structure (b) HLH (continuous line) structure; (c) LML structure; (d) MLM structure.

Our goal is to explore the conditions for resonant OT across different three-layer microsystems, for which we will refer to local transmission maxima as resonances. The permittivity profiles of the structures to be studied here are those depicted in Fig. 1. We have found it appropriate to distinguish dielectric layers with a low refractive index (L) from those with a high refractive index (H).

Let us start by considering a general $\text{SO}_1\text{CO}_2\text{S}$ structure, composed of a core layer C sandwiched between two high-reflectance outer layers O_1 and O_2 , which are embedded in a thick, transparent dielectric surrounding medium, S. The action of the core layer and the outer layers can be separated, so that the latter are characterized by the following amplitude reflection and transmission coefficients:

$$r_{jmk} = \frac{-r_{mj} + r_{mk} e^{i2k_{m\perp} w_m}}{1 - r_{mj} r_{mk} e^{i2k_{m\perp} w_m}} \quad t_{jmk} = \frac{t_{jm} t_{mk} e^{ik_{m\perp} w_m}}{1 - r_{mj} r_{mk} e^{i2k_{m\perp} w_m}} \quad j, k = c, s \quad m = 1, 2 \quad (1)$$

with w_m the width of the outer layer O_m , and $k_{m\perp}$ the component of the wavevector orthogonal to the interfaces inside this layer. There are four coefficients associated with each of these outer layers, namely r_{jmk} , r_{kmj} , t_{jmk} and t_{kmj} . For example, r_{s1c} applies to light incident from the surrounding medium S and reflected by layer O_1 , with the core layer C on the opposite side. Furthermore r_{mj} , r_{jm} , t_{jm} and t_{mj} are the Fresnel reflection and transmission coefficients for incidence at the interface labelled JM. Besides, round-trip propagation in the core layer of thickness d adds the factor $e^{ik_{c\perp} d} / (1 - r_{c1s} r_{c2s} e^{i2k_{c\perp} d})$ to the field, where $k_{c\perp} = k'_{c\perp} + ik''_{c\perp}$ is the transversal component of the wavevector in the core layer. Taking all together, the transmission amplitude coefficient for the three-layer structure is obtained:

$$t_{s1c2s} = \frac{t_{s1c} t_{c2s} e^{ik_{c\perp} d}}{1 - r_{c1s} r_{c2s} e^{i2k_{c\perp} d}} \quad (2)$$

The transmittance of the complete $\text{SO}_1\text{CO}_2\text{S}$ is then straightforwardly calculated as $T = |t_{s1c2s}|^2$. To facilitate the physical interpretation of the subjacent OT process, transparent systems will be addressed first, and the effect of absorption will be incorporated later. In a transparent layer ‘ j ’, the wavevector component in the direction normal to the interfaces can be either real ($k_{j\perp} = k'_{j\perp}$) or imaginary ($k_{j\perp} = ik''_{j\perp}$). In the former case, there are harmonic waves inside the layer, whereas in the latter case there are evanescent waves. In contrast, in the surrounding semi-infinite media S there are always travelling harmonic waves.

There are two types of resonant OT effects that can be distinguished depending on the type of waves allowed in the core layer. Let us consider harmonic waves first, which corresponds to the case of a Fabry-Perot (F-P) etalon, where the transmittance is well-known to be:

$$T = \frac{T_0}{1 + F \sin^2 \left(k'_{c\perp} d + \frac{\varphi_{c1s} + \varphi_{c2s}}{2} \right)} \quad (3a)$$

$$T_0 = \frac{(1 - R_1)(1 - R_2)}{\left(1 - \sqrt{R_1 R_2}\right)^2}; \quad F = \frac{4\sqrt{R_1 R_2}}{\left(1 - \sqrt{R_1 R_2}\right)^2} \quad (3b)$$

in which $R_m = |r_{cms}|^2$ is the reflectance of the outer layer O_m for light travelling inside the core layer, and φ_{cms} is the phase of the amplitude coefficient r_{cms} . $T = T_0$ is the maximum transmittance—and thus its value at resonance—and F is called the finesse, which are both increasing with the reflectance of the outer layers. In particular, for a symmetric system ($\text{O}_1 \equiv \text{O}_2$) such as those in Fig.1(a), $T_0 = 1$ and $F = 4 R_1 / (1 - R_1)^2$.

Provided that the resonances are defined as local maxima of the transmittance, the resonant condition can be obtained by cancelling the sine in Eq. (3):

$$2k'_{c\perp} d + \varphi_{c1s} + \varphi_{c2s} = 2\pi q \quad q \in \mathbb{Z}^+ \quad (4)$$

In this relation the value of d is not limited. However, since we are only interested in optical microstructures, the core layer thickness d will be restricted here to the micron range. The number of resonances depends on the value of $k'_{c\perp} d$, and it is limited to a few units within that range of thicknesses.

As noted, F-P etalons or interferometers constitute the traditional example of an optical system where this type of resonant OT arises. An alternative modern example⁷ features a double barrier photonic structure comprising low-refractive index dielectric outer layers, located between high-index core layer and surrounding medium. The case of interest is that of incidence angles θ from the surrounding larger than the critical angles θ_{cr}^{km} ($m = 1, 2$, $k = c, s$), defined as a function of the corresponding refractive indices by $\sin\theta_{cr}^{km} = n_m / n_k$. In that scenario, waves inside the low-index outer layers are evanescent, with an imaginary wavevector component in the direction normal to the interfaces (let us remember that we are considering harmonic waves inside the core layer). This assures high reflectance for the SO_mC subsystems alone, which is only limited by FTIR. As a consequence, the transmittance of the whole system at resonance and the finesse are also high, until the opaque-layer limit ($R \rightarrow 1$) is achieved. This phenomenon can be called resonant FTIR. Amazingly, this resonant OT effect is more prominent for thicknesses of the outer layer where usual FTIR is reduced.

The transmittance of a symmetric system that features resonant FTIR is shown in Fig. 2, as a function of the wavelength and the incidence angle (the F-P etalon is omitted, since it is well known). The core layer and the surrounding media are both made of TiO₂, $n(589 \text{ nm}) \approx 2.61$, while the outer layers are SiO₂ glass, $n(589 \text{ nm}) \approx 1.46$. It corresponds to the permittivity profile depicted in Fig. 1a. The results shown correspond to transverse electric (TE) polarized waves, but similar ones are obtained for transverse magnetic (TM) polarization. Two different regions can be visually distinguished within the map, below and above the spectral curve of critical angle, $\theta_{cr}(\lambda)$, for the TiO₂ - SiO₂ interfaces. On the one hand, below $\theta_{cr}(\lambda)$, there is high transmittance of white light, which presents some typical modulations due to interference effects. On the other hand, above $\theta_{cr}(\lambda)$, the OT resonances arise, exhibiting a broader spectral width, that means low finesse, the closer to the critical angle curve. That bandwidth reduces as the angle of incidence increases, so that resonances show a higher finesse at larger angles. Indeed, the resonances seem to have disappeared for incidence angles greater than 60°, but that is merely an artifact resulting from the limited resolution of the graph.

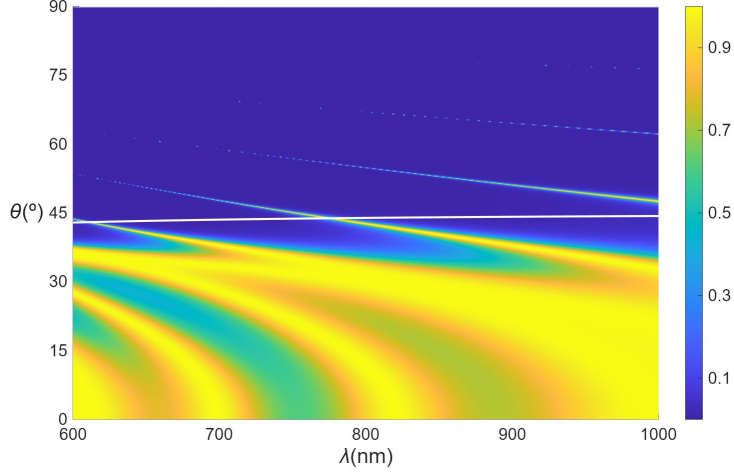


Fig. 2 Transmittance map (λ , θ) for TE waves at a TiO_2 - SiO_2 - TiO_2 - SiO_2 - TiO_2 structure with core layer thickness 800 nm and 400 nm -thick outer layers. The white line corresponds to the spectral curve of the critical angle, $\theta_{cr}(\lambda)$.

Up to now, we have considered resonant OT effects such that waves inside the core layer are harmonic. Let us now address the other case, in which evanescent waves are allowed inside the core layer. Under these conditions, Eq. (2) leads to the following transmittance:

$$T = \frac{T_0}{1 + F \sinh^2(k''_{c\perp} d - 0.5 \ln|r_{c1s}r_{c2s}|)} \quad (5a)$$

$$T_0 = \frac{|t_{s1c}t_{c2s}|^2}{4|r_{c1s}r_{c2s}| \sin^2\left(\frac{\varphi_{c1s} + \varphi_{c2s}}{2}\right)}; \quad F = \frac{1}{\sin^2\left(\frac{\varphi_{c1s} + \varphi_{c2s}}{2}\right)} \quad (5b)$$

Note that, in contrast to Eq. (3), the maximum transmittance T_0 and the finesse F are not written here in terms of the reflectance of the outer layers $R_m = |r_{cms}|^2$ because this concept becomes meaningless when there are evanescent waves in the first medium of the associated amplitude reflection coefficient. The expression for T_0 can be simplified if the conservation of flux in transparent systems is considered, which results in $|t_{s1c}t_{c2s}|^2 = 4|r_{c1s}r_{c2s} \sin \varphi_{c1s} \sin \varphi_{c2s}|$, and thus:

$$T_0 = \frac{|\sin \varphi_{c1s} \sin \varphi_{c2s}|}{\sin^2\left(\frac{\varphi_{c1s} + \varphi_{c2s}}{2}\right)} \quad (6)$$

where the phases of the amplitude reflection coefficients φ_{c1s} and φ_{c2s} are constrained to the interval $[0, \pi]$, so that T_0 meets its maximum value $T_0 = 1$ for $\varphi_{c1s} = \varphi_{c2s}$. Moreover, the denominator of T in Eq. (5) has a minimum when the argument of the hyperbolic sine vanishes, leading to $T = T_0$. As a result, the system will show unitary transmission if these two conditions are satisfied simultaneously:

$$d = \frac{1}{2} \ln|r_{c1s}r_{c2s}|/k_{c\perp}'' \equiv D(\lambda, \theta) \quad (7a)$$

$$\varphi_{c1s}(\lambda, \theta) = \varphi_{c2s}(\lambda, \theta) \quad (7b)$$

Condition (7a) means a maximum in transmittance, i.e. a resonance, while condition (7b) assures unitary transmission at resonance. This last condition is always met for symmetric structures, but it can only be fulfilled for some values of (λ, θ) in the case of asymmetric arrangements. Hence, not all solutions of Eq. (7a) can be considered as proper resonances, since the corresponding value of T_0 could be small. Conversely, some situations can be considered as resonances even if Eq. (7a) is not satisfied. For example, in a symmetric structure, for a constant $\lambda = \lambda_0$, a resonant branch in the (d, θ) plane with $T = T_0 = 1$ corresponds to points in which Eq.(7a) is fulfilled until $D(\lambda_0, \theta)$ reaches its maximum value $D_{max} = D(\lambda_0, \theta_m) = d_m$. For $d > d_m$, the resonance persists at the same angle θ_m , but transmission becomes lower as the core layer thickness grows, since that increases the argument of the sinh function in Eq. 5(a). In short, any resonance must approximately satisfy Eq. (7a) and (7b) but can be extended sometimes to situations in which at least one of the two conditions is not verified.

Furthermore, since d and $k_{c\perp}''$ are both positive, the following condition is necessary for the verification of Eq. (7a):

$$G(\lambda, \theta) = |r_{c1s}r_{c2s}| > 1 \quad (8)$$

This condition is precisely the opposite of the usual case with harmonic waves in the core and surroundings in which the coefficients are roots of a reflectance, and thus lower than unity. Here, the inequality limits the number of configurations for which resonant OT is possible. Some of these configurations correspond to the permittivity profiles shown in Fig. 1(b-d). Only symmetric structures are considered, since they allow unitary transmission. Expressions for $G(\lambda, \theta)$ in each case are given in table 1. Note that metals have been considered ideal, with a negative real dielectric constant.

Table 1. Expressions for $G(\lambda, \theta) = |r_{c1s}r_{c2s}|$ for the three last configurations shown Fig. 1.

Config.	Conditions	$G(\lambda, \theta) = r_{c1s}r_{c2s} $
1(b) TE/TM Waves	$r_{c1s} = r_{c2s}$ $\theta > \theta_c = \sin(n_c/n_s)$ $r_{1s} = \pm \rho_{1s}, \rho_{1s} \leq 1$ $r_{1c} = e^{i\varphi_{1c}}$	$1 - \frac{4\rho_{1s} \sin(2k_{1\perp}'' w_1) \sin(\varphi_{1c})}{(1 - \rho_{1s})^2 + 4\rho_{1s} \sin^2(k_{1\perp}' w_1 + \varphi_{1c}/2)}$
1(c) and 1(d) TM waves	$r_{c1s} = r_{c2s}$ $\theta > \theta_c = \sin(n_1/n_s)$ 1(c) $\theta > \theta_c = \sin(n_c/n_s)$ 1(d) $r_{1c} = \pm \rho_{1c}, \rho_{1c} \geq 1$ $r_{1s} = e^{i\varphi_{1s}}$	$1 + \frac{(\rho_{1c}^2 - 1)(1 - e^{-4k_{1\perp}'' w_1})}{(1 - \rho_{1c} e^{-2k_{1\perp}'' w_1})^2 + 4\rho_{1c} e^{-2k_{1\perp}'' s_1} \sin^2(\varphi_{1s}/2)}$

First, Fig. 1b corresponds to a configuration with a low refractive index dielectric core layer. The outer layers are made of a material with a high refractive index (HLH structure), higher than that of the surrounding medium. In this configuration, Eq. (8) is only verified for some continuous values of θ and λ , depending on the signs of the sine functions in the expression of $G(\lambda, \theta)$. For instance, for a constant incidence angle, θ_0 , $G(\lambda, \theta_0)$ oscillates periodically, alternating zones with values smaller and greater than 1. The greatest and lowest values of $G(\lambda, \theta)$ are achieved for grazing incidence, for which $\rho_{1s} \rightarrow 1$.

An example of an $D(\lambda, \theta)$ map corresponding to this kind of structure is shown in Fig. 3a, together with the transmittance map for the same structure, SiO_2 - TiO_2 - air - TiO_2 - SiO_2 , in Fig. 3(b-c). Following the shape of $G(\lambda, \theta)$, the function $D(\lambda, \theta)$ is sharply peaked near grazing incidence, with pronounced maxima and minima. If we follow the curve for each maximum or minimum, $|D(\lambda, \theta)|$ decreases as θ does. However, it increases again near the critical angle, due to the greater value of $1/k_{c\perp}''$.

The transmittance maps in Fig. 3(b) corresponds to those configurations with core layer thicknesses of $d = 150 \text{ nm}$. A series of double resonances can be seen near grazing incidence, each of which degenerates into a single resonance for lower incidence angles. These resonance branch shapes are related to those of the $D(\lambda, \theta)$ patterns in Fig. 3a. The merging into a single resonance is accompanied by a reduction in transmittance, since Eq. (7a) is no longer fulfilled. T increases again as θ approaches θ_{cr} , since $D(\lambda, \theta)$ approaches

d again. This map includes transmittance for $\theta < \theta_{cr}$, where resonances are F-P type and verify Eq. (4). A very different behaviour appears in fig. 3(c) where we show transmittance for this kind of structure with $d = 450 \text{ nm}$. Whereas the number of resonances above the critical angle is the same, because such number is determined by the product $k''_{m\perp} s_m$, and thus by the thickness of the outer layers, the transmittance at resonances decreases with the thickness d of the core layer. In contrast, the number of resonances of F-P type, i.e. for angles below $\theta_{cr}(\lambda)$, varies. This happens because it depends on the product $k'_{c\perp} d$, and therefore on the thickness of the core layer. However, note that in both cases there is a smooth transition of transmittance at the frontier of the two regimes.

Lastly, we note that a different variant of this resonant OT arises when the dielectric in the core layer of this structure is replaced by a metallic layer⁸.

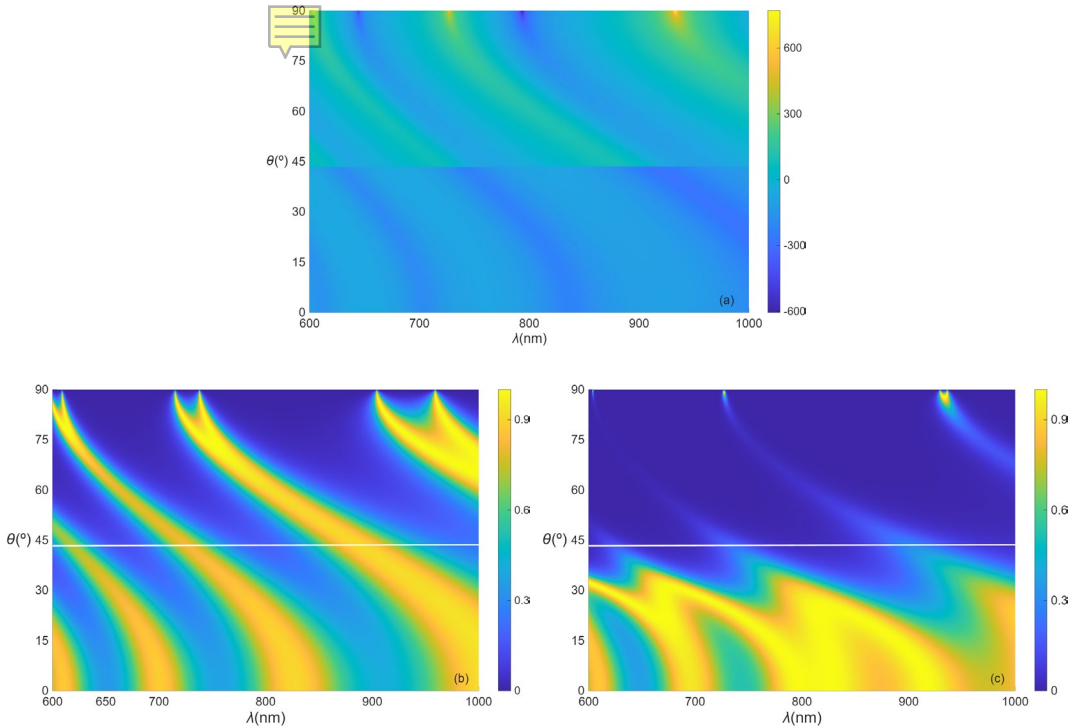


Fig. 3. (a) Map of function $D(\lambda, \theta)$ for TE waves in a $\text{SiO}_2 - \text{TiO}_2 - \text{Air} - \text{TiO}_2 - \text{SiO}_2$ configuration with $w_m = 1000 \text{ nm}$. Transmittance map for this structure with a core layer thickness of $d = 150 \text{ nm}$ (b) and $d = 450 \text{ nm}$ (c). The white line corresponds to the spectral curve of the critical angle, $\theta_{cr}(\lambda)$. While all the figures are plotted for angles between 0° and 90° , the information in (a) below $\theta_{cr}(\lambda)$ is not relevant

The next cases to be studied are those displayed in Fig. 1c and 1d, which are obtained from one another by interchanging the core and outer layers. The former corresponds to an LML

multilayer, where a metallic core layer is sandwiched between two dielectric layers with a refractive index lower than that of the surrounding medium S. The latter, in turn, corresponds an MLM multilayer.

Indeed, the expression for $G(\lambda, \theta)$ is identical in both cases, as indicated in table 1. As listed in this table, $G(\lambda, \theta) > 1$ above the critical angle (for $\theta > \theta_c$) in any case for TM waves, since $\rho_{1c} > 1$. However, Eq. (8) is never satisfied in the case of TE waves, for which $\rho_{1c} < 1$. The resonances in these configurations are related to the generation of coupled surface plasmons (CSP)^{13,23}. $G(\lambda, \theta)$ and transmittance maps (λ, θ) for an example of each of the two structures are shown in Fig. 4.

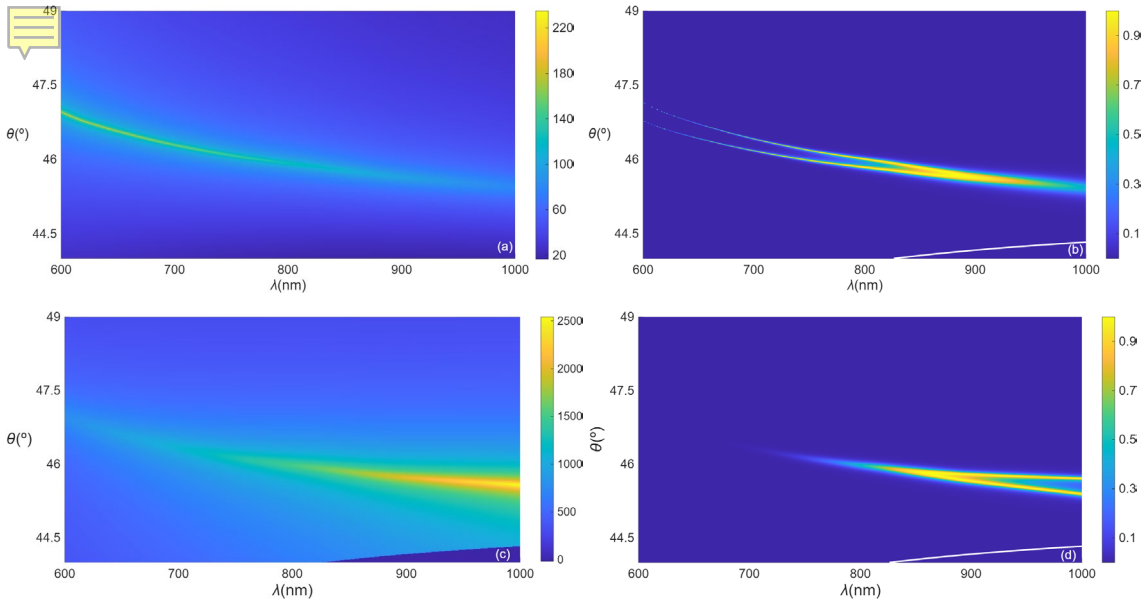


Fig. 4. $G(\lambda, \theta)$ (a) and transmittance (c) for an $\text{TiO}_2\text{-SiO}_2\text{-Ag}^*\text{-SiO}_2\text{-TiO}_2$ structure (Ag^* stands for ideal Ag metal, i.e. with a real permittivity) with $w_m = 900 \text{ nm}$ and $d = 100 \text{ nm}$. $G(\lambda, \theta)$ (b) and transmittance (d) for a $\text{TiO}_2\text{-Ag}^*\text{-SiO}_2\text{-Ag}^*\text{-SiO}_2$ structure with $w_m = 50 \text{ nm}$ and $d = 1800 \text{ nm}$. The white lines in (c) and (d) correspond to the spectral critical angle curve $\theta_{cr}(\lambda)$.

In both LML and MLM cases represented in Figs. 4(a) and 4(b), $G(\lambda, \theta)$ is observed to have a single branch of high value, beginning at larger incidence angles and shorter wavelengths, and progressing toward smaller incidence angles and longer wavelengths. Given that $k_{c\perp}''$ is a monotonically increasing function of θ , $D(\lambda, \theta)$ will also have a local maximum for each λ along a similar curve in the (λ, θ) plane. Let us denote this curve as $D_{max}(\lambda, \theta)$. For wavelengths such that $D_{max} > d$, Eq. (7a) will be satisfied at two points, located on either

side of D_{max} , leading to two branches of maximum unitary transmission (remember that Eq. 7(b) is always fulfilled for symmetric systems). Otherwise, for other wavelengths $D_{max} < d$ and, in that zone, the two resonances in transmittance degenerate into a single resonance curve. Along this curve, T is now smaller since Eq.(7a) is not fulfilled because $D(\lambda, \theta)$ does not reach d for any resonance angle θ .

The most significant difference regarding transmittance for the two structures lies on the spectral regions where the two resonant branches remain distinct or are merged into a single curve. In LML systems (Fig. 4a and 4c), the maximum of $G(\lambda, \theta)$ is higher for shorter wavelengths and larger incidence angles. This leads to a higher D_{max} and thus to two different resonances within that zone, which become degenerated for longer wavelengths. In contrast, the reverse situation occurs in MLM systems (Fig. 4b and 4d), where the greater maximum of $G(\lambda, \theta)$ and the separated resonances occur for longer λ and smaller θ . Another remarkable difference is that MLM systems admit F-P type resonances for $\theta < \theta_{cr}(\lambda)$, while LML systems do not. Indeed, in MLM systems there is a maximum transmittance branch that crosses $\theta_{cr}(\lambda)$, as can be seen in Fig. 4d. This is referred to as the hybrid resonance, since it is of F-P type below $\theta_{cr}(\lambda)$ and plasmonic in nature above it.

So far, we have considered ideal transparent media. Let us now deal with lossy metals in what follows. Typically, metals in the visible range exhibit a complex dielectric constant, whose real part is negative and greater in magnitude than the imaginary part, i.e. $\varepsilon = \varepsilon' + i\varepsilon''$, where $-\varepsilon' \gg \varepsilon'' > 0$. This affects resonant optical tunnelling in plasmonic configurations (Fig 1 (c-d)), which are the only ones that include metals among the considered arrangements. On the one hand, in this situation, the resonant conditions in Eq. (7), remain valid. However, the position of the resonances changes since $\varepsilon'' \neq 0$ affects the expression of the reflection coefficients r_{c1s}, r_{c2s} . However, given that $-\varepsilon' \gg \varepsilon''$, this change is rather small.

On the other hand, the expression for T_0 in Eq. 6 must be modified to account for absorption. Limited by that process, unitary transmission is no longer possible. Therefore, we call this phenomenon attenuated optical tunnelling (AOT). Obviously, this imposes limitations on the thickness of the metallic layers within the structure. Maximum transmission values for various examples of the studied structures LMH and HML with varying metallic thicknesses are shown in Fig. 5. For low thickness the transmission is small since there is not sufficient distance to develop the resonance ($d < D_{min}(\lambda, \theta)$). In the case of a metallic core layer, the highest transmission maximum is achieved near 20-25 nm. This peak in maximum

transmission is followed by a decay that shows an initial approximately linear trend, which becomes exponential for thicker metal layers. In the case of a dielectric core the highest transmission maximum decreases with wavelength, while the corresponding metallic thickness increases with wavelength. At sufficiently short wavelengths, the chosen core thickness exceeds $D_{max}(\lambda, \theta)$, and, consequently, the transmission becomes smaller and smaller

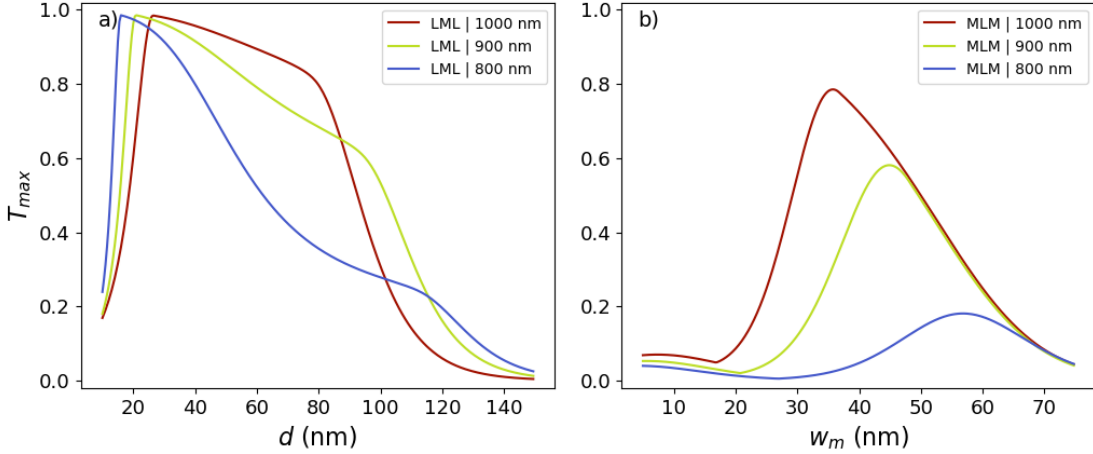


Figure 5. Maximum transmittance value of plasmonic resonances for LML a) ($\text{TiO}_2\text{-SiO}_2\text{-Ag-SiO}_2\text{-TiO}_2$) and MLM b) ($\text{TiO}_2\text{-Ag-SiO}_2\text{-Ag-TiO}_2$) arrangements, as function of the metallic thickness, for 3 different wavelengths. The thickness of the L layer is $w_m = 900$ nm for LML and $d = 1800$ nm for MLM structures.

In the case of dielectric layers, absorption does not play a relevant role. However, limitations on the width of the tunneled layers due to the skin depth values must be considered. Let us consider first the LHL multilayer, Fig 1(a). For thicknesses within or below the order of the skin depth, the outer layers exhibit moderate reflectance because of FTIR, resulting in broad, low-contrast resonances. As the width of the outer layers increases, their reflectance approaches one, and the resonances become finer. As shown in ^{24,25}, in the opaque limit ($R_j \rightarrow 1, j = 1, 2$), tunneling times are inversely proportional to transmittance ($T_j = 1 - R_j$). Thus, the first outer layer blocks the beam and allows for no tunneling flux. Nevertheless, this is not expected to occur until tunneling layer thickness reach several wavelengths.

On the other hand, resonances in HLH structures are wide and limited to nearly grazing incidence angles. Therefore, we will not discuss this type of structure further here.

Considering the plasmonic structures, those involving metals, the limit on the width of their dielectric layers is related to the maximum of the D function in Eq. 7(a), $D_{max}(\lambda, \theta)$, which is associated as well with the unusually high value of the maximum in $G(\lambda, \theta)$. Considering for example the MLM structure, for $d < D_{max}(\lambda, \theta)$ the system achieves a maximum transmittance of T_o , as commented above, only limited by absorption. And for $d > D_{max}(\lambda, \theta)$, the transmittance decreases as thicknesses increase. However, at the same time the maximum of T_o decreases with the of the maximum in $G(\lambda, \theta)$ ¹³. Therefore, in AOT, there is always a compromise between high transmittance and the high thickness that allows the phenomenon to occur. For example, Fig. 5 shows that high transmittances, above 50 % despite Ag absorption, can be easily achieved for thicknesses of the dielectric layers larger than various wavelengths.

Summary

Up to four three-layer configurations for resonant OT, always embedded in a high-index thick media (which can be considered as semi-infinite), have been analysed. Namely, LHL, HLH dielectric structures and LML, MLM structures including metallic layers, have been studied. The first structure differs from the others in both its expression for transmittance and the derived resonance condition (based on phase). This is a consequence of the waves within the core layer being harmonic instead of evanescent or damped, as in the rest of the cases. The two first configurations, consisting only of dielectric layers differ notably in the finesse of their resonances, which are very fine for LHL structures and much broader for HLH arrangements. Moreover, the number of resonances is related to the width of the core layer in the former case, and to the width of the outer layers in the latter. In the two last configurations, OT is associated with the generation of CSP resonances, so that there are only two resonances that slowly merge into one as the thickness of the core layer d increases. For sufficiently large thickness, OT vanishes due either to absorption in the metallic layers or to total reflection at the first outer layer. Finally, it has been shown that while absorption limits the width of the metallic layers to tens of nanometres, the thickness of the tunnelled dielectric layers can achieve over-wavelength values.

Funding

This research was funded through projects by the Spanish Ministry of Science, Innovation and Universities (PID2024-156552OA-I00), Universidade de Santiago de Compostela (USC 2024-PU031) and Xunta de Galicia (GRC ED431C 2024/06), respectively. Finally, AD thanks the Spanish Ministry of Science, Innovation and Universities for the financial support through FPU21/01302, as well as YA acknowledges Xunta de Galicia for the postdoctoral fellowship ED481D-2024-001.

Data Availability Statement

The data that support the findings of this study are available from the corresponding author upon reasonable request.

Conflicts of interest

The authors declare that they have no known competing financial interests or personal relationships that could have appeared to influence the work reported in this paper.

References

1. Chiao, R. Y., Kwiat, P. G. & Steinberg, A. M. Analogies between electron and photon tunneling. *Physica B: Condensed Matter* **175**, 257–262 (1991).
2. Wave optics versus wave mechanics I. in *Introduction to Nanophotonics* (ed. Gaponenko, S. V.) 35–78 (Cambridge University Press, Cambridge, 2010). doi:10.1017/CBO9780511750502.004.
3. Jian, A. *et al.* Optical and quantum models of resonant optical tunneling effect. *Optics Communications* **428**, 191–199 (2018).
4. Riga, J. & Sevior, R. Electromagnetic analogs of quantum mechanical tunneling. *Journal of Applied Physics* **132**, 200901 (2022).
5. Cluzel, B. & De Fornel, F. Frustrated total internal reflection: the Newton experiment revisited. *Photoniques* 32–37 (2022) doi:10.1051/photon/202211632.

6. Born, M. & Wolf, E. *Principles of Optics: Electromagnetic Theory of Propagation, Interference and Diffraction of Light*. (Cambridge University Press, Cambridge, 1999). doi:10.1017/CBO9781139644181.
7. Hayashi, S., Kurokawa, H. & Oga, H. Observation of Resonant Photon Tunneling in Photonic Double Barrier Structures. *Optical Review* **6**, 204–210 (1999).
8. Hooper, I. R., Preist, T. W. & Sambles, J. R. Making Tunnel Barriers (Including Metals) Transparent. *Phys. Rev. Lett.* **97**, 053902 (2006).
9. Jian, A. Q. & Zhang, X. M. Resonant Optical Tunneling Effect: Recent Progress in Modeling and Applications. *IEEE J. Select. Topics Quantum Electron.* **19**, 9000310–9000310 (2013).
10. Dragila, R., Luther-Davies, B. & Vukovic, S. High Transparency of Classically Opaque Metallic Films. *Phys. Rev. Lett.* **55**, 1117–1120 (1985).
11. Wakamatsu, T. Characteristics of Metal Enhanced Evanescent-Wave Microcavities. *Sensors* **10**, 8751–8760 (2010).
12. Yoshida, M., Tomita, S., Yanagi, H. & Hayashi, S. Resonant photon transport through metal-insulator-metal multilayers consisting of Ag and SiO_2 . *Phys. Rev. B* **82**, 045410 (2010).
13. Doval, A., Arosa, Y. & de la Fuente, R. Coupled surface plasmons and resonant optical tunnelling in symmetric optical microcavities. *Optics & Laser Technology* **192**, 113602 (2025).
14. Allen, T. W. & DeCorby, R. G. Conditions for admittance-matched tunneling through symmetric metal-dielectric stacks. *Opt. Express* **20**, A578 (2012).
15. Zhang, M. C., Allen, T. W. & DeCorby, R. G. Experimental study of optimized surface-plasmon-mediated tunneling in metal-dielectric multilayers. *Appl. Phys. Lett.* **103**, 071109 (2013).

16. Orlov, A. A., Zhukovsky, S. V., Iorsh, I. V. & Belov, P. A. Controlling light with plasmonic multilayers. *Photonics and Nanostructures - Fundamentals and Applications* **12**, 213–230 (2014).
17. Davidovich, M. V. Resonant Tunneling of Photons in Layered Optical Nanostructures (Metamaterials). *Tech. Phys.* **69**, 1521–1530 (2024).
18. Liu, W.-C. & Tsai, D. P. Optical tunneling effect of surface plasmon polaritons and localized surface plasmon resonance. *Phys. Rev. B* **65**, 155423 (2002).
19. Zhou, L., Wen, W., Chan, C. T. & Sheng, P. Electromagnetic-Wave Tunneling Through Negative-Permittivity Media with High Magnetic Fields. *Phys. Rev. Lett.* **94**, 243905 (2005).
20. Ebbesen, T. W., Lezec, H. J., Ghaemi, H. F., Thio, T. & Wolff, P. A. Extraordinary optical transmission through sub-wavelength hole arrays. *Nature* **391**, 667–669 (1998).
21. Barnes, W. L., Murray, W. A., Dintinger, J., Devaux, E. & Ebbesen, T. W. Surface Plasmon Polaritons and Their Role in the Enhanced Transmission of Light through Periodic Arrays of Subwavelength Holes in a Metal Film. *Phys. Rev. Lett.* **92**, 107401 (2004).
22. García De Abajo, F. J., Gómez-Santos, G., Blanco, L. A., Borisov, A. G. & Shabanov, S. V. Tunneling Mechanism of Light Transmission through Metallic Films. *Phys. Rev. Lett.* **95**, 067403 (2005).
23. Welford, K. R. & Sambles, J. R. Coupled Surface Plasmons in a Symmetric System. *Journal of Modern Optics* **35**, 1467–1483 (1988).
24. Winful, H. G. Apparent superluminality and the generalized Hartman effect in double-barrier tunneling. *Phys. Rev. E* **72**, 046608 (2005).
25. Xiao, Z., Huang, H. & Lu, X.-X. Resonant tunneling dynamics and the related tunneling time. *Int. J. Mod. Phys. B* **29**, 1550052 (2015).

